Biofilm Development in a Membrane-Aerated Biofilm Reactor: Effect of Flow Velocity on Performance

Eoin Casey, Brian Glennon, Geoffrey Hamer

Chemical Engineering Department, University College Dublin (UCD),

Belfield, Dublin 4, Ireland; telephone: +353 1 706 1824; fax: 353 1 706 11 77

Abstract: The effect of liquid flow velocity on biofilm development in a membrane-aerated biofilm reactor was investigated both by mathematical modeling and by experiment, using *Vibrio natriegens* as a test organism and acetate as carbon substrate. It was shown that velocity influenced mass transfer in the diffusion boundary layer, the biomass detachment rate from the biofilm, and the maximum biofilm thickness attained. Values of the overall mass transfer coefficient of a tracer through the diffusion boundary layer, the biofilm, and the membrane were shown to be identical during different experiments at the maximum biofilm thickness. Comparison of the results with published values of this parameter in membrane attached biofilms showed a similar trend. Therefore, it was postulated that this result might indicate the mechanism that determines the maximum biofilm thickness in membrane attached biofilms. In a series of experiments, where conditions were set so that the active layer of the membrane attached biofilm was located close to the membrane biofilm interface, it was shown that the most critical effect on process performance was the effect of velocity on biofilm structure. Biofilm thickness and effective diffusivity influenced reaction and diffusion in a complex manner such that the yield of biomass on acetate was highly variable. Consideration of endogenous respiration in the mathematical model was validated by direct experimental measurements of yield coefficients. Good agreement between experimental measurements of acetate and oxygen uptake rates and their prediction by the mathematical model was achieved.

INTRODUCTION

In the study of biofilm reactor performance, the effect of flow velocity is mainly of interest with regard to mass transfer by diffusion in the boundary layer at the biofilm liquid interface and on detachment rates. However, the flow velocity can also influence the formation of biofilms and their structure. Numerous recent studies have shown that biofilms can no longer be considered to be homogeneous structures (Costerton et al., 1994; DeBeer et al., 1994), and this has an important role in the analysis of biofilm reactor performance. However, to date there seems to be no generally accepted theory describing how the effect of flow velocity influences the formation of different biofilm structures.

In membrane-attached biofilms, where limiting substrates are supplied from opposite sides of the biofilm, and where the active layer is not necessarily located adjacent to the biofilm–liquid interface, the effects of biofilm structure, and the resultant changes in effective substrate diffusivities, can have a critical influence on process performance. The effects of flow velocity on a membrane-aerated biofilm have been considered previously by Debus et al. (1994) when it was shown that the average flow velocity affected the diffusion boundary layer thickness, the biofilm density, and detachment rate. However, quantitative measurements of the biofilm density were not reported, and a constant effective diffusion coefficient for substrates in the biofilm was assumed for mathematically modeling the system.

This paper seeks to examine the performance characteristics of membrane-aerated biofilms during their development under different flow conditions. In order to fully consider the effects of biofilm structure and the mass transfer resistance during diffusion in the boundary layer, operating parameters such as the carbon substrate concentration and the intra-membrane oxygen pressure were chosen so that the active layer would be located adjacent to the biofilm– membrane interface rather than at the biofilm–liquid interface, i.e., high carbon substrate concentrations and low intra-membrane oxygen pressures. Since the carbon substrate must be transported through the boundary layer, whose mass transfer resistance is related to the flow velocity and, also, through the entire biofilm depth, whose mass transfer resistance is related to biofilm structure, the effects of velocity and structure can be observed simultaneously. A mathematical model for performance of the membrane aerated biofilm reactor (MABR) incorporating the effect of endogenous respiration and using in situ measurements of the effective diffusivity of substrates in the biofilm is compared with experimental observations of the reaction rates

of the limiting substrates and with biomass yield coefficients

MATERIALS AND METHODS

Bioreactor Configuration

The general scheme of the MABR system used has been described previously by Casey et al. (1999a). Figure 1 shows an outline of the experimental apparatus. The aerobic halotolerant acetate-utilizing bacterium, *Vibrio natriegens,* was used in this study under non-aseptic conditions. The medium composition used was that given previously by Casey et al. (1999a) where it was shown that *V. natriegens* behaves as an obligate aerobe when acetate is used as the carbon source.

Analytical Methods

The oxygen transfer rate through the membrane was measured using the technique proposed by Eberhard and Schügerl (1986). High sensitivity in this measurement was achieved by the use of a model PS100GC pressure transducer (Sensortechnics, Pucheim, Germany) connected to a chart recorder. The system was calibrated by measuring the oxygen concentration in the off-gas of the STR by gas chromatography when the reactor system was operated without biofilm. The biofilm thickness was measured using the non- invasive and nondestructive technique developed by Freitas dos Santos and Livingston (1995a). The estimated error in the measurement at the magnification used in the experiments was typically ±20 µm. The average biofilm thickness was measured at different points along the length of the membrane module. A gas chromatograph with a thermal conductivity detector (Gow-Mac, Shannon, Ireland) with parallel columns packed with 5 Å molecular sieves and Poropak Q was used to measure the concentrations of carbon dioxide, oxygen and nitrogen in the off gases of both the membrane lumen and the STR. Suspended cell concentration in the liquid effluent was estimated after measuring dry weights of samples filtered through 0.20 µm membranes (Whatman, Maidstone, U.K.). The average biofilm density at the end of each experiment was measured by removing all biofilm from the membrane and drying at 100°C for 24 h.

All carbon flows were balanced assuming that removed carbon substrate that does not

exit the reactor as either CO_2 or as bicarbonate is retained as biofilm carbon. CO_2 concentrations in the exit gases from the membrane lumen, the stirred tank reactor (STR) headspace and the total inorganic carbon (TIC) concentration in the liquid effluent were measured. Dissolved inorganic carbon in the effluent was measured using a photometric technique, which relates the quantity of CO_2 evolved after reagent has been added to a sample (Dr. Lange, Düsseldorf, Germany).

MABR Operation

When the membrane was initially pressurized with oxygen, even at low pressures, oxygen bubbles tended to form on the membrane. Within a day of growth medium recirculation (without either inoculum or carbon source addition), the oxygen bubbles were completely removed. After inoculation, the growth of suspended culture was encouraged by conventional bubble aeration in the STR up to the point where the batch culture was growing exponentially and the dry weight in the culture had reached approximately 50 mg/L. At this point, a base film of cells had formed on the membrane. Liquid medium aeration was then ceased, nitrogen gas was sparged into the liquid in the STR to discourage suspended growth in the liquid and to encourage biofilm growth on the membrane and the bioreactor was switched from batch operation to continuous flow medium feeding. Suspended cells were quickly washed out of the system. This start-up procedure resulted in visible "patchy" biofilm growth on the membrane after only a few hours, but after 10–20 h, it was observed that the entire membrane was covered with an evenly distributed thin biofilm. Three series of experiments, corresponding to average flow velocities of 2, 6, and 12 cm s^{-1}, respectively, were conducted. The nutrient medium feed rate to the bioreactor was maintained constant at 110 mL/h and a fixed feed concentration of 430 mg/L acetate was used throughout all experiments. The pH was maintained at 7.0, and the temperature was controlled at 30°C during all experiments.

Diffusion Coefficient Measurement

The method described by Zhang et al. (1998), using nitrogen as the tracer component, was used to measure the diffusion coefficients of substrates in the biofilm. It was assumed that nitrogen influences neither microbial reaction nor endogenous processes. The growth medium in the STR was continuously bubbled with nitrogen for the purposes of preventing

suspended cell growth, to allow off gas measurement of oxygen and to achieve effective mixing. Under the operating conditions used in this study, the liquid was saturated with nitrogen, and since the membrane lumen oxygen partial pressure was always greater than 98% of the total pressure, there was a strong concentration gradient between the liquid phase and the gas phase in the membrane lumen. Eq. (1) shows the main resistances to mass transfer of the tracer, and Fig. 2 shows schematically the profile of the resistances to mass transfer

$$\frac{1}{k_{\mathrm{O}}} = \frac{r_{\mathrm{M}} \ln\left(\frac{r_i}{r_{\mathrm{M}}}\right)}{P_{\mathrm{M,N2}} H_{\mathrm{N2}}} + \frac{r_{\mathrm{M}} \ln\left(\frac{r_i + \delta}{r_i}\right)}{D_{\mathrm{e,N2}}} + \frac{r_{\mathrm{M}}}{(r_i + \delta) k_{\mathrm{L,N2}}}. \qquad (1)$$

In order to determine the mass transfer coefficient of the membrane wall, experiments were conducted without biofilm. The values obtained were found to differ from those based on calculations from published data for membrane permeability. It has been suggested by Cote (1989) that such published permeability data should only be used as an approximation because of differences in the composition of silicone from different manufacturers. Therefore, in this study, experimentally determined membrane permeabilities have been used. The diffusivity of nitrogen in water and Henry's law constants for nitrogen–water were obtained from Perry and Green (1997). The concentration of nitrogen in the membrane lumen was determined by gas chromatography and the concentration gradient of nitrogen for calculation of the overall mass transfer coefficient was calculated as a logarithmic mean difference. As shown by Zhang et al. (1998) Eq. (1) can be rearranged to give Eqs. (2)–(4):

$$\gamma = \frac{\varepsilon}{D_{\mathrm{e,N2}}} + \frac{1}{k_{\mathrm{L,N2}}}, \qquad (2)$$

Where

$$\gamma = \left(\frac{1}{k_O} - \frac{r_M \ln\left(\frac{r_i}{r_M}\right)}{P_{M,N2} H_{N2}} \right) \frac{(r_i + \delta)}{r_M}, \qquad (3)$$

and

$$\varepsilon = (r_i + \delta) \ln\left(\frac{r_i + \delta}{r_i}\right). \qquad (4)$$

A plot of γ versus ε gives a straight line, the slope of which is the reciprocal of the effective diffusion coefficient. The effective diffusion coefficient of nitrogen in the biofilm is related to the diffusion coefficient in water by means of an effective diffusion factor, and this in turn is used to calculate the effective diffusion coefficients of substrates such as oxygen and acetate in the biofilm. The intercept of the γ versus ε plot is inversely proportional to the mass transfer coefficient of the tracer in the boundary layer at the biofilm– liquid interface. The mass transfer coefficient of acetate in the boundary layer at the biofilm–liquid interface was related to the measured mass transfer of nitrogen by the ratio of the diffusivities of the two components to the power of two thirds (Cussler, 1989), i.e.,

$$\frac{k_{L,Act}}{k_{L,N2}} = \left(\frac{D_{Act}}{D_{N2}} \right)^{2/3}. \qquad (5)$$

In an MABR it was hypothesized by Casey et al. (1999a) that three layers exists with respect to the two limiting substrates, oxygen and acetate. Figure 3 shows schematically the acetate-depleted layer, the oxygen-depleted layer, and the growth layer. The configuration of the layers in the MABR is unique in that the carbon substrate-starved layer adjacent to the membrane is oxygen-rich and provides an environment where oxygen can be utilized for "endogenous reactions" such as the oxidation of cell storage products and cell leakage products and the breakdown of extracellular polysaccharides. This layer is termed the "endogenous" layer. In this communication the diffusion and

reaction of the two limiting substrates is modeled by considering the reactions occurring in two layers of the stratified biofilm, i.e., the growth layer and the endogenous decay layer. It has been shown previously by Casey et al. (1999a) that *V. natriegens* behaves as an obligate aerobe when acetate is the sole carbon source and, therefore, it is assumed that no reaction occurs in the oxygen depleted layer adjacent to the liquid. A further assumption of the model is that "cryptic" growth can be incorporated into endogenous decay as far as its overall effects are concerned, i.e., yield coefficient reduction.

The growth reaction is:

$$CH_3COO^- + 0.16O_2 + 0.37NH_3 \rightarrow 1.39CH_{1.8}O_{0.5}N_{0.2} + 0.51CO_2 + 0.72H_2O. \quad (6)$$

The endogenous decay reaction is:

$$CH_{1.8}O_{0.5}N_{0.2} + 1.05O_2 \rightarrow CO_2 + 0.6H_2O + 0.2NH_3 \quad (7)$$

The model is similar in form to that described by Pavasant et al. (1997) for an extractive membrane bioreactor, but the method adopted for solution is different. MABR performance has previously been modeled by Casey et al. (1999a) considering only the growth reaction by adapting a model proposed by Karel and Robertson (1987) for co-substrates diffusing from opposite sides of a catalyst. However, in the model described here, the Karel and Robertson (1987) model (referred to here as the "growth only model") is only one step in the solution of a combined model of growth and endogenous decay. Here, in addition to prediction of the reaction rates for limiting substrates and active layer location, the model was extended to allow estimation of the yield coefficient, $Y_{X/S}$, for formation of biomass from acetate. If it is assumed that biomass resulting from the growth reaction has an ash free elemental composition of $CH_{1.8}O_{0.5}N_{0.2}$ and that cell material involved in the endogenous respiration reaction has the same elemental composition then, depending on the relative rates of the two reactions (Eq. 6 and 7) an observed value of $Y_{X/S}$ can be calculated. The algorithm for the numerical solution is described in the Appendix and the parameters used in the model are given in Table I.

RESULTS

Physical Effects: Thickness, Structure, Mass Transfer, and Detachment

Biofilm Thickness Development

Biofilm average thickness was measured daily during biofilm buildup for each 10–12 day experiment. Reported values of the biofilm thickness refer to the average of twenty measurements taken at the top, middle, and bottom of the membrane biofilm module. No significant axial gradient with respect to thickness was observed. Figure 4 shows the development of biofilm thickness with respect to time, where it can be seen that the biofilm growth rate was independent of the liquid medium flow velocity except in the case of run 3 (12 cm s^{-1}) where a rapid increase in biofilm thickness between days two and four was followed by significant sloughing of biomass. Recovery of the biofilm after sloughing was rapid, and as can be seen in Fig. 4, the growth continued at a similar rate in all three experiments. The actual value of the steady state thickness was dependent on the liquid velocity with the greatest steady state thickness occurring at the lowest velocity.

Biofilm Detachment Rate

As the average thickness approached the steady state value, a noticeable increase in the effluent suspended cell concentration was observed. This phenomenon can be attributed to erosion as opposed to sloughing and corresponds to a situation where biofilm growth is balanced by biofilm removal at the steady state thickness. Figure 5 shows the specific detachment rates of biomass over the course of biofilm development during each experiment. There is a clear dependence of velocity (shear rate) on detachment. However, the specific detachment rate was not constant during each experiment suggesting that factors other than the shear rate are involved in detachment.

Effective Diffusivity of Substrates

The technique of Zhang et al. (1998) was used to determine the diffusion coefficients of substrates in the biofilm and the mass transfer coefficients at the biofilm–liquid interface. Figure 6 show the plots of the parameters γ against ε, defined by Zhang et al. (1998) which

were used to calculate these parameters. Shear rate or velocity is generally accepted to exert a strong effect on biofilm structure and the results presented in this paper confirm this view. Values of the effective diffusion coefficients determined from the slopes of the plots in Fig. 6 are summarized in Table II together with estimated values of the experimental error. The results show that biofilms formed under conditions of high velocity result in structures that present a significant mass transfer resistance to substrates. The opposite is the case for conditions of low flow velocity where a more open, loose structure was visually observed and where high substrate diffusion coefficients through the biofilm were measured. Biofilm density was determined at the end of each experiment, and in order to investigate if there was a relationship between substrate diffusion coefficients and the biofilm density, the final biofilm density was plotted against the final effective diffusivity in Fig. 7. This plot allows comparison of the present results with the extensively used density–diffusivity correlation proposed by Fan et al. (1990). The experimental data are not in good agreement with the proposed correlation because use of such a model assumes that density is the only factor controlling the mass transfer of solutes in biofilms. At the microscopic scale, the structure of a biofilm is complex, a feature discussed in more detail below.

Diffusion Boundary Layer

The measured values of the diffusion boundary layer thickness are plotted in Fig. 8 as a function of velocity. In addition, values of the mass transfer coefficient determined by the use of oxygen microelectrodes, that have been reported in the literature, are also shown.

Although there is significant scatter in the data, a general trend, which is in good agreement with the literature values, can clearly be observed. Scatter in the data may be attributed to the effects of different surface roughness properties of the biofilms, a feature which is believed to affect the mass transfer coefficient but which is difficult to measure directly.

Performance Effects: Substrate Uptake, Yield Coefficients, and Location of the Active Layer

The predicted location of the active layer of biomass within the membrane immobilized biofilm is plotted in Fig. 9 as a function of biofilm thickness, in terms of the parameter v,

with $l < v < \lambda$, where the biofilm–membrane interface has a value 1 and the biofilm–liquid interface is represented as A, defined by λ

$$\lambda = \frac{(r_i + \delta)}{r_i}. \qquad (8)$$

The measured uptake of the two limiting substrates, acetate and oxygen, are plotted in Figs. 10a and 11a against the average biofilm thickness. From the mathematical model, the predicted trends in acetate removal rate and the oxygen uptake rate are shown in Figs. 10b and 11b and show qualitatively the correspondence with the experimentally observed trends.

Effect of Biofilm Thickness on Substrate Removal Rates

In all three experiments, the results show a general trend of decreasing substrate uptake rates as the biofilm thickness develops despite an increasing liquid–biofilm interfacial area. During experiments at flow velocities of 2 and 6 cm s^{-1}, sudden decreases in the acetate removal rate occurred when the biofilm thickness exceeded "critical" values of 1100 and 1000 μm, respectively. These changes in performance in each experiment corresponded to a simultaneous and marked change in substrate effective diffusivity which, as can be seen from Table II occurs at biofilm thicknesses of about 1300 and 1100 μm, respectively.

Effect of Velocity on the Acetate Removal Rates

Figure 10a shows that for a fixed biofilm thickness the flow velocity has a significant effect on the acetate removal rate. Results for biofilm thicknesses below 100 μm in each experiment will not be discussed here due to the possible interfering effects of suspended cell reactions during the initial biofilm startup. However, between biofilm thicknesses of 100 and 1000 μm, Fig. 11 shows that velocity had a "negative" influence on reaction rate, i.e., the highest acetate removal rates occurred at the lowest velocities. This result is counterintuitive when one considers that higher velocities enhance mass transfer through the diffusion boundary layer. However, the effect can be explained by considering that during these experiments, first, flow velocity affected the biofilm structure and second, the active layer within the biofilm was located adjacent to the membrane–biofilm interface. In these experiments, mass transfer was limited by the diffusive

resistance in the biofilm itself, rather than diffusion through the boundary layer, and since the biofilms formed a more open structure during development under low flow velocity conditions, higher acetate uptake rates resulted. Between 1000 μm and the maximum biofilm thickness, there was no clear trend between velocity and acetate removal rate due to changes in biofilm structure during experiments at 2 and 6 cm s^{-1} because the relationship between flow velocity and effective diffusivity was different to that observed for thinner biofilms. When the biofilm thickness had reached particular steady state values, the highest acetate removal rate occurred at the highest velocity, a completely opposite effect to that observed for thinner biofilms.

Oxygen Uptake Rate

Figure 11 shows that in the case of experiments at 2 and 6 cm s^{-1} and thicknesses of above 1000 μm, the acetate removal rate falls to very low values (0.05–0.10 mmol h^{-1}) compared to values in thinner biofilms (up to 0.60 mmol h^{-1}). However, in thick biofilms the oxygen uptake rate values can be seen to be high (ca. 0.15 mmol h^{-1}) compared to their maximum values (0.25–0.30 mmol h^{-1}) in thin biofilms. An explanation for this is that although oxygen is one of the limiting substrates, it differs from acetate in that oxygen is utilized during both growth and endogenous respiration. During dual limitation, the operating regime predominating in all experiments in this paper, oxygen is transported through an acetate-depleted layer (the endogenous layer) of the biofilm between the membrane and the active (growth) layer. If the acetate removal rate is low, or even zero, it can be hypothesized that a certain quantity of oxygen will continue to be transferred through the membrane for use in endogenous respiration. Such a hypothesis is supported by the results shown in Fig. 11a where an asymptotic value of the oxygen uptake rate is reached with increasing biofilm thickness, regardless of the acetate removal rate. In order to confirm if all transferred oxygen is consumed in the biofilm, measurements of oxygen concentration in the off- gas of the STR were measured and found to be zero.

Biomass Yield Coefficient

Predictions of the biomass yield coefficient are compared to the experimental measurements in Fig. 12. The relative thickness of the various layers existing in the biofilm has a

significant effect on the biomass yield coefficient. In Fig. 12 the observed yield coefficient is plotted against the acetate removal rate and it can be seen from both the experimental and the modeled results that low $Y_{X/S}$ values are observed at low acetate removal rates. When the growth layer thickness is large relative to the endogenous layer thickness, the observed yield coefficient approaches its maximum value. However, when the endogenous layer thickness is large relative to the growth layer, higher oxygen consumption in the endogenous layer relative to the growth layer results in a minimization of the yield coefficient and a concomitant reduction in the acetate removal rate.

DISCUSSION

The success of the mathematical model in predicting trends in the experimental results may be attributed to the inclusion of two important effects. First, the high oxygen uptake rates and low biomass yield coefficients in thick diffusion-limited biofilms highlighted the need to include endogenous respiration reactions in the mathematical model. Second, the marked effect of flow velocity on biofilm structure was considered in the model by using only measured values of the effective diffusivity of substrates.

A combination of physical and physiological processes including attachment, cell growth, endogenous decay, and detachment (erosion or sloughing) determine biofilm development. As demonstrated by the results shown in Figs. 10 and 11, the MABR and indeed other forms of membrane- attached biofilms (Freitas dos Santos et al., 1995b) differ from conventional biofilms in that biofilm thickness can limit reactor performance as a result of diffusional limitations. Therefore, the ability to manipulate biofilm thickness is critical for optimizing the operation of such systems. Possible mechanisms suggested for maximizing performance are the control of biomass detachment rate (Debus et al., 1994) and the ability to manipulate conditions so that endogenous decay may largely balance cell growth (Pavasant et al., 1996). There is no generally accepted theory for biofilm detachment. The model of Rittman (1982) assumes that detachment is purely a physical process determined by the biofilm thickness, its density, and the imposed shear stress. However, Peyton and Characklis (1993) have shown that detachment rate is independent of shear stress and proposed a kinetic expression that indicates a dependence exists with respect to the substrate utilization rate, the yield coefficient, and the biofilm thickness. At a controlled shear stress, nutrient limitations have been shown to increase the detachment rate (Sawyer and Hermanowicz, 1998). Recently, it

has been suggested that attachment and detachment of cells to and from biofilms may be regulated by their physiology, and it has been shown that freely diffusable chemical signals in the form of *N*-acyl homoserine lactones (HSLs) influence the development and maintenance of Gram-negative biofilms (Davies et al., 1998). These HSLs have been shown to influence the formation of *Pseudomonas fluorescens* biofilms (Allison et al., 1998), but not necessarily cell detachment. However, it has also been shown by Allison et al. (1998) that cell detachment from biofilms may be influenced by enzymatic degradation of exopolymers and that such enzymes may be produced as a response to environmental factors such as oxygen starvation. The results presented in Fig. 5 show a marked difference in the detachment rate during each experiment, which may be due to either different growth rates or degrees of nutrient limitation, rather than being necessarily due to different shear stresses. The detachment process is clearly a complex problem, which is not facilitated by the difficulty of conducting experiments where shear stress can be varied independently of the growth rate of the component organisms of the biofilm. Further work needs to be done before detachment phenomena can be defined and integrated into biofilm models. In these experiments a clear point is reached where biofilm thickness stops increasing. This is termed the steady state biofilm thickness even if the biofilm is not necessarily at a steady state with respect to other parameters. There is no accepted theory that describes a mechanism for the attainment of a particular steady state thickness in either conventional biofilms or membrane attached biofilms. Figure 13 summarizes data from Casey et al. (1999b), and the present results for experiments where both intra-membrane oxygen pressure and liquid flow velocity were varied and where the overall mass transfer coefficient of a tracer was measured.

It can be seen that, in all five experiments, as the biofilm thickness developed toward its maximum value, that $k_{O,N2}$ never fell below a critical value of ca. 1.2×10^{-6} m s^{-1}, and that this critical value was the same in all five experiments regardless of the experimental conditions employed. Furthermore, examination of a similar figure in a recent paper of Zhang et al. (1998) also shows that the final value of the overall mass transfer coefficient of the tracer was almost identical in two different experiments. These results suggest a possible mechanism that controls maximum biofilm thickness in membrane-attached biofilms, i.e., that biofilm thickness and structure development in such biofilms occurs until a certain critical overall mass transfer coefficient is reached.

The biomass yield coefficient was shown to be dependent on the relative rates of oxygen respiration in the growth layer to that in the endogenous layer. In the experiments reported in

this communication, the active layer was located relatively close to the membrane, indicating that the endogenous layer was rather thin. Nonetheless, low yield coefficients were observed particularly when the biofilms was thick and the effective diffusivity was low. Yield coefficient minimization is one the objectives of effective aerobic biological wastewater treatment processes. The possibilities of carbon substrate removal with zero or close to zero sludge production was discussed by Tijhuis et al. (1994) when it was shown that the maintenance concept (Pirt, 1965) was applicable in biofilm airlift suspension reactors. For low specific substrate loading rates in such reactors, it was possible to minimize the biomass yield coefficient when the substrate loading was just enough to generate the energy needed for maintenance purposes. In experiments with a three-phase fluidized bed bioreactor Ritmann et al. (1992) measured the active fraction of biomass by use of the INT test (Zimmermann et al., 1978). As would be expected, the active fraction increased with increasing substrate flux as deeper penetration into the biofilm occurred. Decreasing the substrate flux increased the inactive fraction, and it was also observed that the overall biomass yield coefficient decreased due to endogenous respiration in the inactive fraction of the biofilm. Figure 12 shows that in MABRs that biomass yield coefficients can be minimized. However, although the mechanisms responsible for this are the same as those for similar effects in conventional biofilms, the conditions under which such processes occur are more complex but most probably more easily subject to control.

CONCLUSIONS

Flow velocity had a strong influence on a number of parameters. In an MABR under conditions where the active layer was located close to the membrane biofilm interface the effect of velocity on biofilm structure was critical as far as process performance was concerned. Velocity also had an effect on mass transfer by diffusion through the boundary layer, on the detachment rate, and on the maximum biofilm thickness. When biofilm thickness was high and substrate limitation occurred, the acetate removal rate was reduced while oxygen uptake rate remained relatively high and the yield of biomass on acetate was minimized. Such an effect was attributed to endogenous respiration, and this hypothesis was confirmed not only by direct experimental measurements of yield coefficients but also by the good agreement that occurred between experimental results and predictions from a mathematical model that incorporated the endogenous respiration reaction. Values for the overall mass transfer coefficient of a tracer through the diffusion boundary layer, the biofilm, and the membrane during different experiments were shown to be identical at the maximum

biofilm thickness. Comparison with published values of this parameter in membrane attached biofilms showed a similar trend. It was postulated that this result may indicate a mechanism that determines the maximum biofilm thickness that can occur in membrane- attached biofilms.

APPENDIX

Solution of the Mathematical Model

In MABRs, oxygen limitation occurs when the active layer is located adjacent to the membrane. It can be shown that for a given set of parameters, there exists a critical oxygen concentration at the membrane–biofilm interface, below which oxygen limitation is encountered. In this case, the endogenous layer thickness is zero and the model solution described in Casey et al. (1999a) can be used. Dual limitation, which in the case of the MABR, means that the active layer is located between the membrane and the liquid, results in oxygen consumption both in the endogenous layer and in the growth layer. The solution to the mathematical model is based on the model of Karel and Robertson (1987) using the same assumptions as those proposed by Casey et al. (1999a) for the MABR system used in these experiments, i.e., zero-order kinetics for both limiting substrates, a steady state with respect to reaction and diffusion and a structurally homogeneous biofilm. However, in the revised model presented here, the boundary of the biocatalyst used was not the entire annular biofilm, but the annular section of biofilm excluding the endogenous layer. Oxygen diffusion and reaction in the endogenous layer were incorporated into the model by use of equations derived by Chang and Moo-Young (1988) with the membrane as an external mass transfer resistance and zero-order kinetics of oxygen consumption. A numerical scheme was set up whereby the boundary of the endogenous growth layer was increased by increments of 1 mm away from the membrane, changing the thickness of the annular biofilm. Oxygen concentrations at the boundary were predicted using the equations of Chang and Moo-Young (1988) and used in the model of Karel and Robertson (1987) to calculate the acetate and oxygen profiles in the biofilm. The reaction rate for growth, $q_{o,g}$, was based on the stoichiometry and maximum growth rate of *V. natriegens*, as given in Casey et al (1999a). The specific oxygen reaction rate in the endogenous layer, $q_{o,e,}$ was obtained from data fitting. Iterations in the endogenous layer thickness were continued until convergence, i.e., when acetate penetrated to a depth in the biofilm corresponding to the interface of the two layers. The acetate and oxygen uptake rates and the biomass yield coefficient were subsequently calculated.

Acknowledgements

Our thanks are due to Kerr-McGee Oil (U.K.) plc. for financial support and also to Messrs. T. Burke, D. Cash, P. O'Halloran, J. Nolan, and L. Morris for equipment construction and technical support.

References

Allison DG, Ruiz B, SanJose C, Jaspe A, Gilbert P. 1998. Extracellular products as mediators of the formation and detachment of Pseudomonas fluoroscens biofilms. FEMS Microbiol Lett 167:179–184.

Casey E, Glennon B, Hamer G. 1999a. Oxygen mass transfer characteristics in a membrane aerated biofilm reactor. Biotechnol Bioeng 62: 183–193.

Casey E, Glennon B, Hamer G. 1999b. Review of membrane aerated biofilm reactors. Resources, Conservation Recycling 27:203–215.

Casey E, Glennon B, Hamer G. 1999c. Biofilm development in a membrane-aerated biofilm reactor: Effect of intra-membrane oxygen pressure performance. Bioproc Eng (accepted).

Costerton JW, Lewandowski Z, De Beer D, Caldwell D, Korber D, James

G. 1994. Biofilms, the customised microniche. J Bacteriol 176: 2137–2142.

Davies DG, Parsek MR, Pearson JP, Iglewski BH, Costerton JW, Greenberg EP. 1998. The involvement of cell-to-cell signals in the development of a bacterial biofilm. Science 280:295–298.

De Beer D, Stoodley P, Roe F, Lewandowski Z. 1994. Effects of biofilm structures on oxygen distribution and mass transport. Biotechnol Bioeng 43:1131–1138.

Debus O, Baumgaertl H, Sekoulov I. 1994. Influence of fluid velocities on the degradation of volatile aromatic compounds in membrane bound biofilms. Water Sci Technol 29(10–11):253–262.

Fan LS, Leyva-Ramos R, Wisecarver KD, Zehner BJ. 1990. Diffusion of phenol through a biofilm grown on activated carbon particles in a draft tube three-phase fluidized bed bioreactor. Biotechnol Bioeng 35: 279–286.

Freitas dos Santos LM, Livingston AG. 1995. Membrane-attached biofilms for VOC wastewater treatment. II: Effect of biofilm thickness on per- formance. Biotechnol Bioeng 47:90–95.

Han P, Bartels DM. 1996. Temperature dependence of oxygen diffusion in H2O and D2O. J Phys Chem 100:5597–5602.

Karel SF, Robertson CR. 1987. Reaction rate calculations for cosubstrates diffusing into catalyst layer from opposite sides. Biotechnol Bioeng 30:427–438.

Pavasant P, Freitas dos Santos LM, Pistikopoulos EN, Livingston AG. 1996. Prediction of optimal biofilm thickness for membrane-attached biofilms growing in an extractive membrane bioreactor. Biotechnol Bioeng 52:373–386.

Perry RH, Green DW. 1997. Perry's chemical engineers handbook. 7th ed. New York:

McGraw-Hill.

Peyton BM, Characklis WG. 1993. A statistical analysis of the effect of substrate utilisation and shear stress on the kinetics of biofilm detachment. Biotechnol Bioeng 41:728–735.

Pirt SJ. 1965. The maintenance energy of bacteria in growing cultures. Proc R Soc Lond Biol 163:224–234.

Rittmann BE. 1982. The effect of shear stress on biofilm loss rate. Biotechnol Bioeng 24:501–506.

Rittmann BE, Trinet F, Amar D, Chang HT. 1992. Measurements of the activity of a biofilm: effects of surface loading and detachment on a three-phase, liquid-fluidized bed reactor. Wat Sci Technol 26(3–4): 585–594.

Sawyer LK, Hermanowicz SW. 1998. Detachment of biofilm bacteria due to variations in nutrient supply. Wat Sci Technol 37(4–5):211–214.

Tijhuis L, van Loosdrecht MCM, Heijnen JJ. 1994. Formation and growth of heterotrophic aerobic biofilms on small suspended particles in airlift reactors. Biotechnol Bioeng 44:595–608.

Zhang S-F, Splendiani A, Freitas dos Santos LM, Livingston AG. 1998.

Determination of pollutant diffusion coefficients in naturally formed biofilms using a single tube extractive membrane bioreactor. Biotechnol Bioeng 59:80–89.

Zimmermann R, Iturriaga R, Becker-Beck J. 1978. Simultaneous determination of the total number of aquatic bacteria and the number thereof involved in respiration. Appl Environ Microbiol 36:926–935.

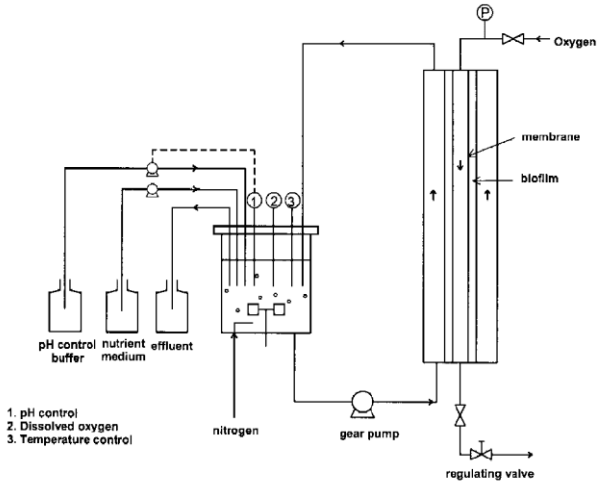

Figure 1 Schematic diagram of the experimental apparatus.

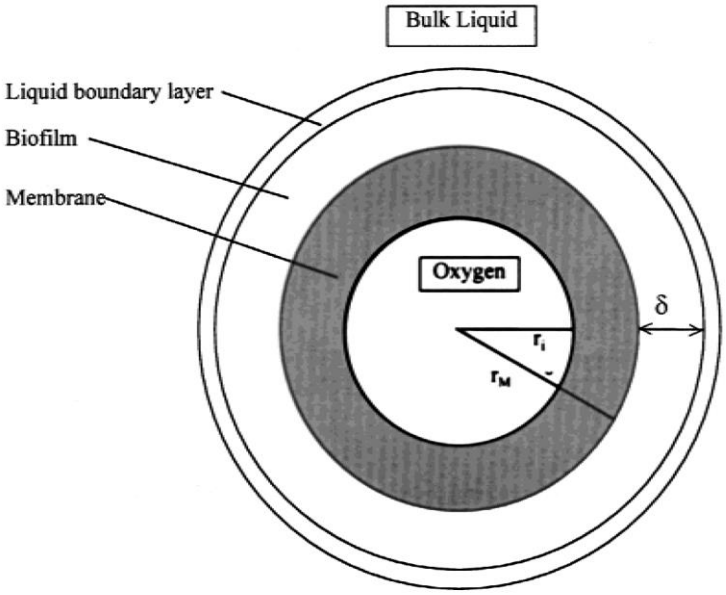

Figure 2 Schematic diagram showing a profile of the membrane and biofilm with the nomenclature used for the diffusion coefficient measurement technique.

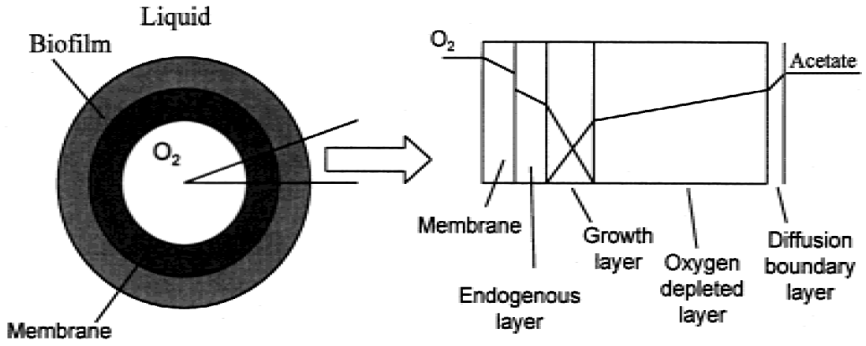

Figure 3 **Figure 3.** Schematic diagram of the MABR showing the various layers in the biofilm and typical concentration profiles of the limiting substrates

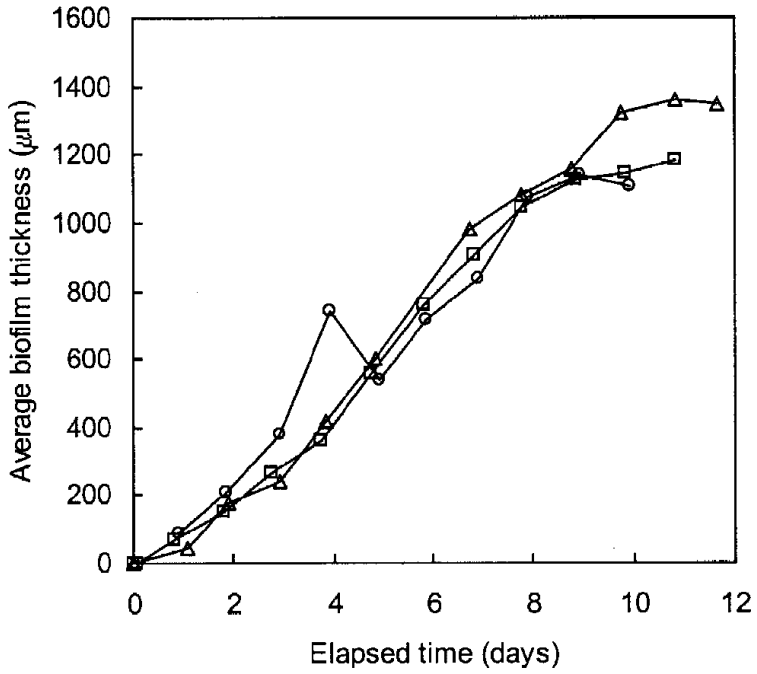

Figure 4. Biofilm thickness development plotted against time for flow velocities of 2 (□), 6 (△), and 12 cm s^{-1} (○).

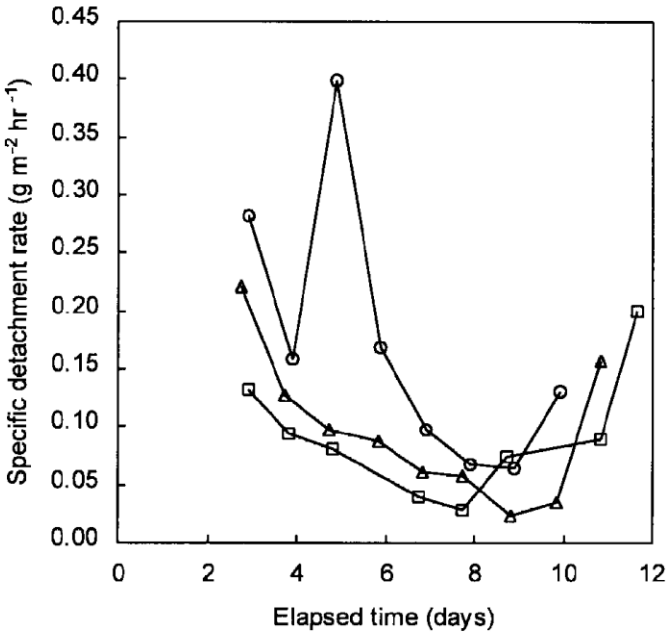

Figure 5. Specific biomass detachment rates during development of biofilms for flow velocities of 2 (□), 6 (△), and 12 cm s^{-1} (○).

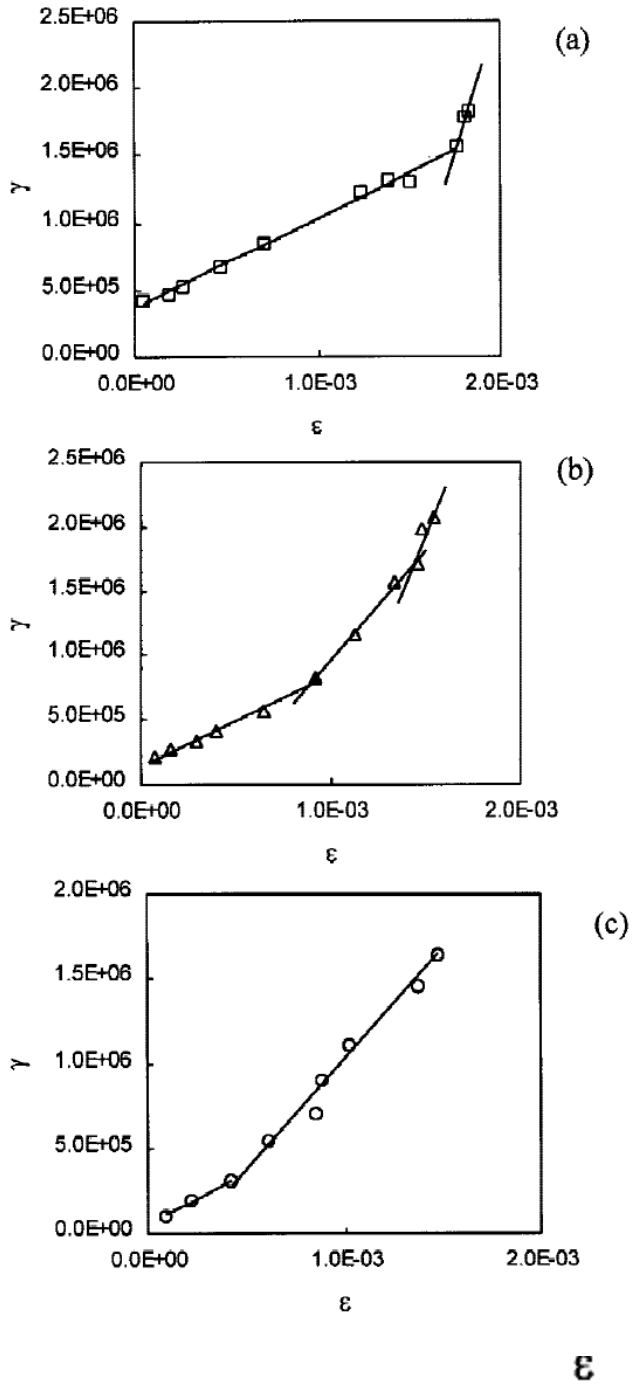

Figure 6. Plots of γ against ε for biofilms formed with flow velocities of 2 (□), 6 (△), and 12 cm s^{-1} (○).

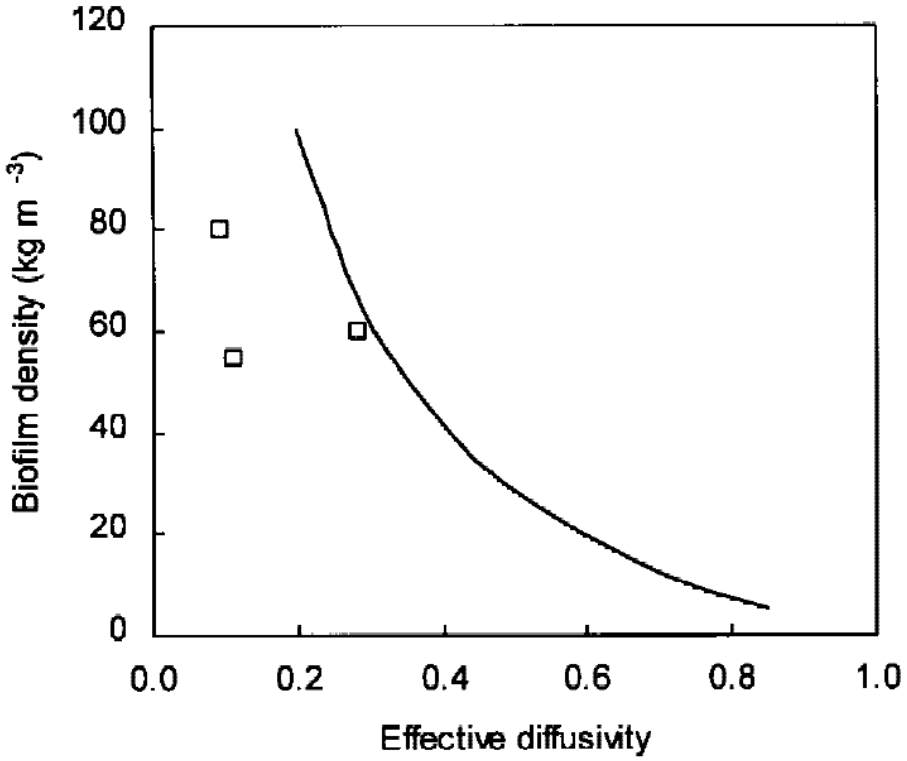

Figure 7. Experimentally observed final biofilm densities plotted against the experimentally determined final effective diffusivities are shown by open squares (□), while results derived from the empirical equation of Fan et al. (1990) are shown as a continuous line.

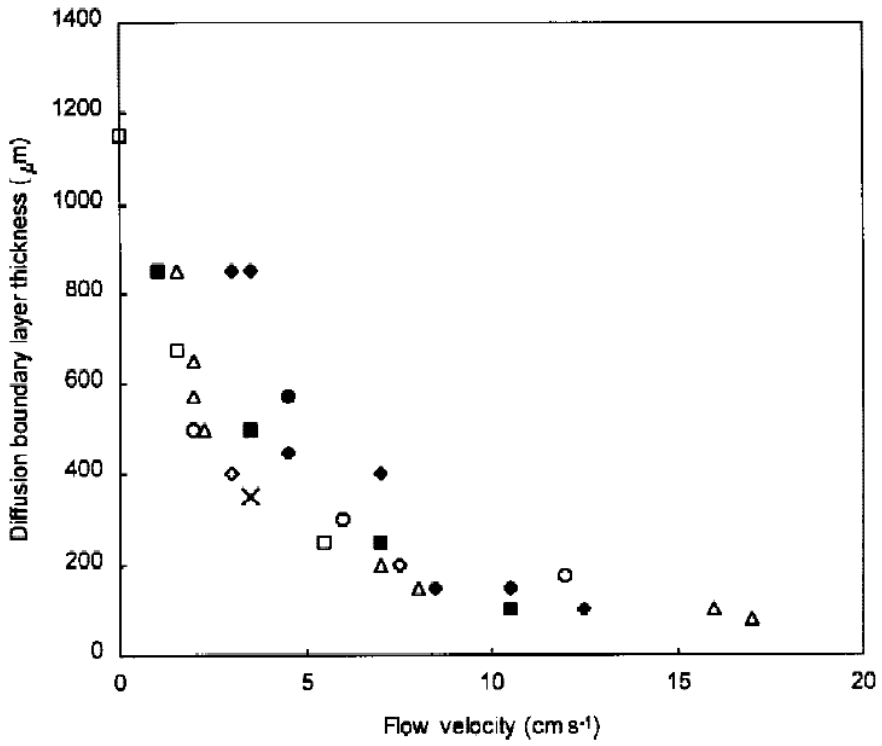

Figure 8. Experimentally determined values of the diffusion boundary layer thickness plotted against the flow velocity and compared to a number of literature values [adapted from Horn and Hempel (1998)]: Kuenen et al. (1986) (◇); Horn (1992) (■); Debus (1993) (●); Lewandowski et al. (1993) (×); Horn and Hempel (1995) (◆); Kuhl et al. (1995) (□); Horn and Hempel (1998) (△); present study (○).

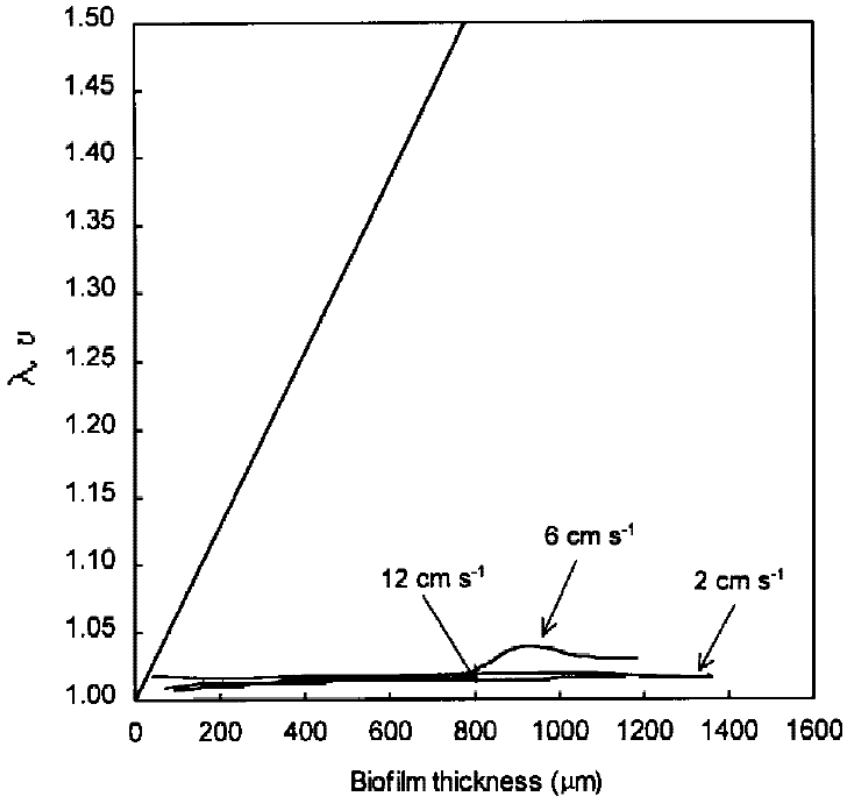

Figure 9. υ, the dimensionless location of the reaction layer plotted against the biofilm thickness, with the dimensionless biofilm thickness, λ, also shown.

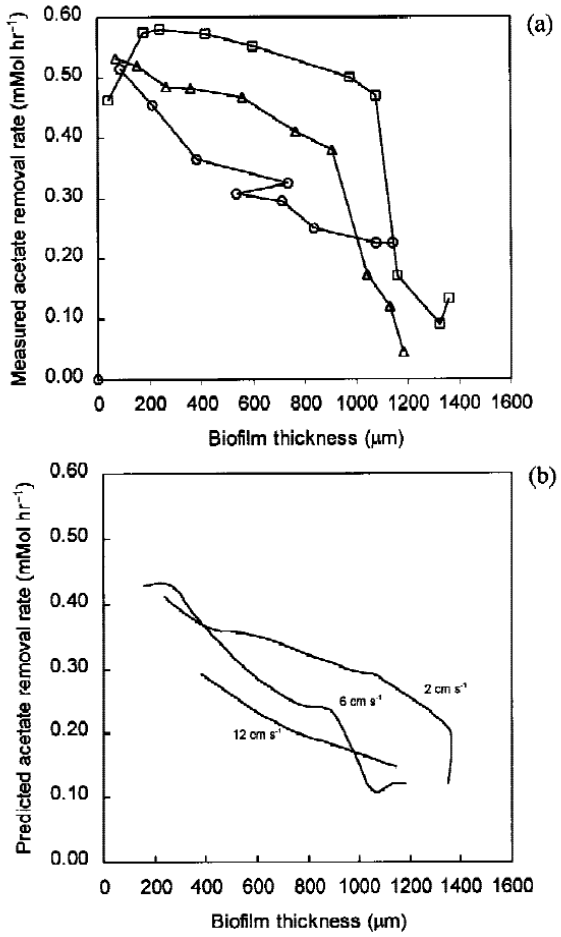

Figure 10. (a) Experimentally observed acetate removal rates plotted against biofilm thickness for flow velocities of 2 (□), 6 (△), and 12 cm s^{-1} (○). Continuous lines represent trends through the data. (b) Model-predicted values of the acetate removal rates plotted against biofilm thickness.

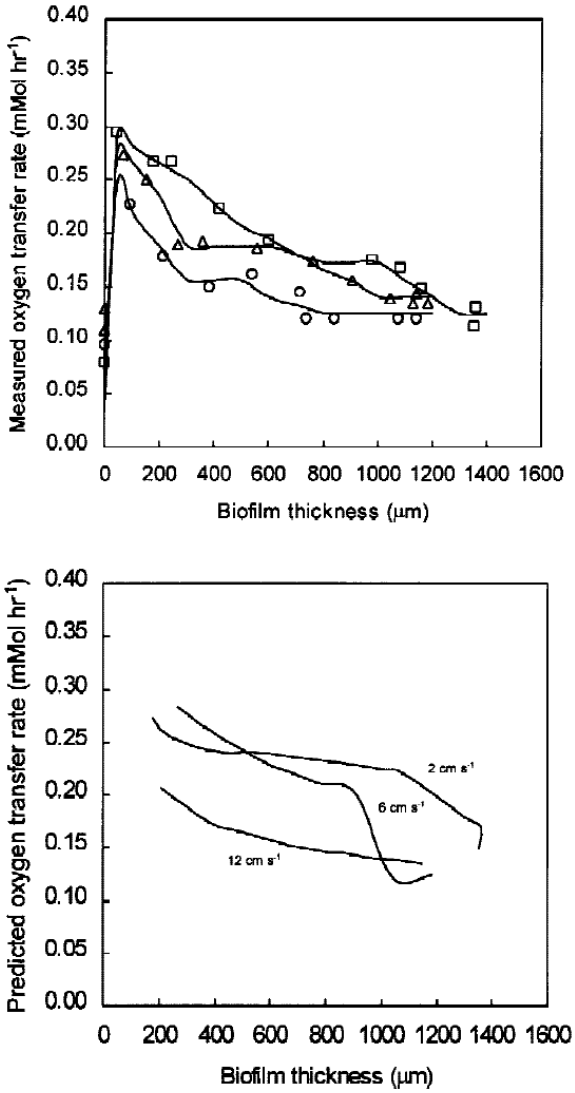

Figure 11. (a) Experimentally observed oxygen uptake rates plotted against biofilm thickness for flow velocities of 2 (□), 6 (△), and 12 cm s^{-1} (○). Continuous lines represent trends through the data. (b) Model-predicted values of the oxygen uptake rates plotted against thickness.

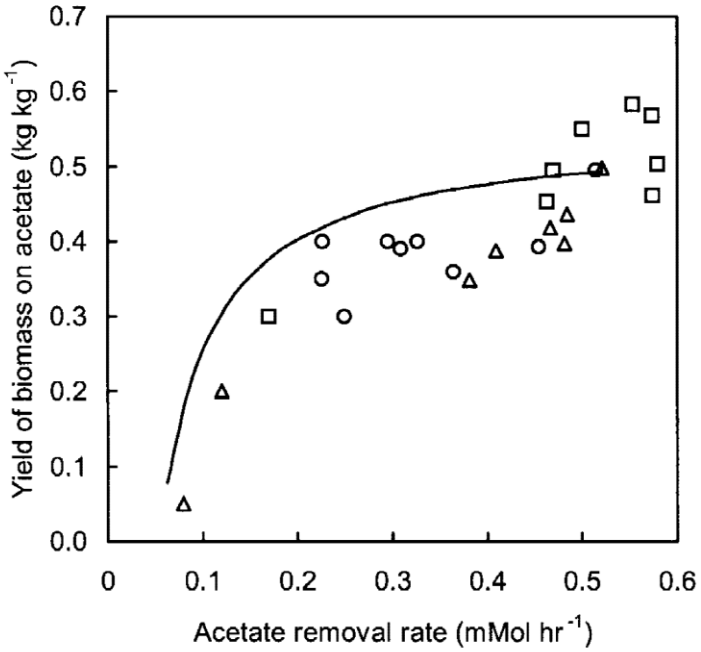

Figure 12. Experimentally observed biomass yield coefficients from acetate for flow velocities of 2 (□), 6 (△), and 12 cm s^{-1} (○). Model-predicted yield coefficients are shown as a continuous line.

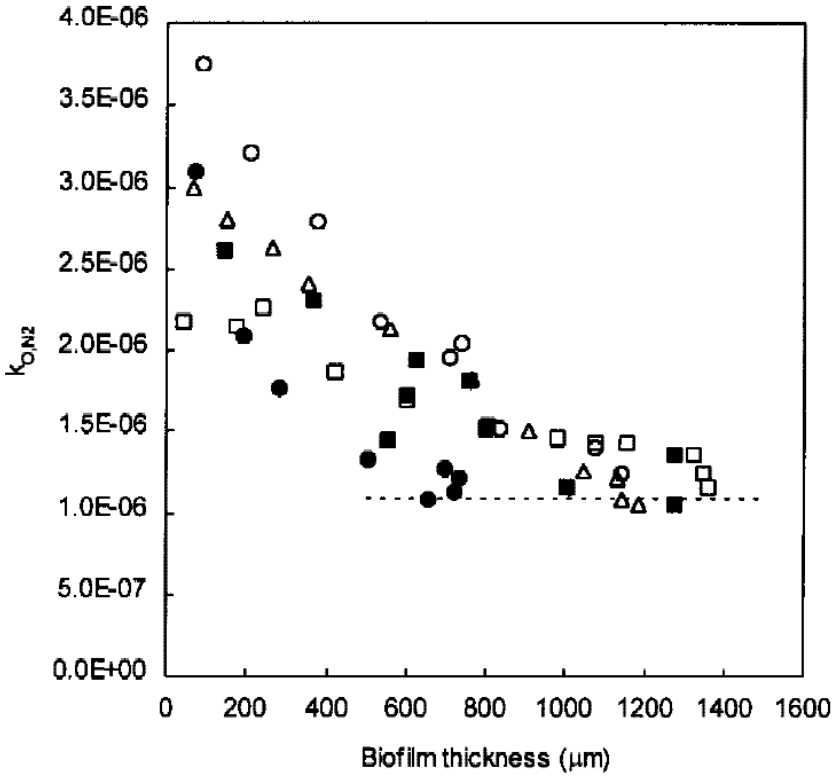

Figure 13. Overall mass transfer coefficient of nitrogen through the membrane, biofilm, and diffusion boundary layer for experiments at a constant intramembrane oxygen pressure of 1.5 kPa and flow velocities of 2 (□), 6 (△), and 12 cm s^{-1} (○) and experiments with a constant flow velocity of 6 cm s^{-1} and intramembrane oxygen pressures of 25 (●) and 50 kPa (■).

Table I. Parameters used in the mathematical model.

Parameter	Value	Source
D_{Act}	1.24×10^{-9} m^2 s^{-1}	Perry and Green (1997)
$D_{e,Act}$	See Table II	This study
D_{N2}	1.90×10^{-9} m^2 s^{-1}	Perry and Green (1997)
D_{O2}	1.19×10^{-9} m^2 s^{-1}	Han and Bartels (1996)
H_{N2}	1.56×10^{5} Pa m^3 mol^{-1}	Perry and Green (1997)
H_{O2}	7.38×10^{4} Pa m^3 mol^{-1}	Perry and Green (1997)
$k_{L,N2}$, $k_{L,Act}$	See Table II	This study
$P_{M,N2}$	7.3×10^{-14} mol m^{-1} s^{-1} Pa^{-1}	This study
$P_{M,O2}$	2.0×10^{-13} mol m^{-1} s^{-1} Pa^{-1}	This study
$q_{o,g}$	0.25 mol m^{-3} s^{-1}	This study
$q_{o,e}$	0.025 mol m^{-3} s^{-1}	Fitted

Table II. Summary of effective diffusivity measurements and mass transfer measurements determined from Fig. 6.

Flow velocity (cm s^{-1})	Biofilm thickness range (μm)	D_{eff}	95% Confidence limit on D_{eff} measurement	r^2	$k_{L,Act}$ (10^{-6} ms^{-1})
2	0 to 1158	0.59	0.06	0.99	1.62
	1158 to 1360	0.09	0.08	0.99	
6	0 to 760	0.57	0.06	0.99	4.03
	760 to 1100	0.24	0.15	0.97	
	1100 to 1184	0.11	0.08	0.71	
12	0 to 380	0.66	0.21	0.99	18.1
	380 to 1141	0.28	0.12	0.94	

Nomenclature

$C_{X,f}$	biofilm density, kg m^{-3}
D	diffusion coefficient in water, m^2 s^{-1}
D_{eff}, D_e	diffusion coefficient in biofilm, m^2 s^{-1}
H	Henry's law constant, Pa m^3 mol^{-1}
k_L	mass transfer coefficient in the concentration boundary layer at the biofilm–liquid interface, m s^{-1}
k_o	overall mass transfer coefficient, m s^{-1}
P_M	membrane permeability, mol m^{-1} s^{-1} Pa^{-1}
$q_{o,g}$	specific oxygen uptake rate for the growth reaction, mol m^{-3} s^{-1}
$q_{o,e}$	specific oxygen uptake rate for the endogenous reaction, mol m^{-3} s^{-1}
r_I	inner radius of membrane, m
r_M	outer radius of membrane, m
r^2	correlation coefficient
$Y_{X/S}$	yield coefficient of biomass on substrate, kg kg^{-1}
δ	biofilm thickness, m
λ	dimensionless biofilm thickness
γ	parameter defined in Eq. (3)
ε	parameter defined in Eq. (4)
ν	dimensionless location of the active biomass layer in the biofilm

Subscripts

Act	acetate
N_2	nitrogen
O_2	oxygen